

This manuscript is a preprint that is currently undergoing peer-review in the *Journal of Natural Gas Science and Engineering*. Subsequent versions of this manuscript may have different content. If accepted, the final version of this manuscript will be available via the Peer-reviewed Publication DOI link on the right-hand side of this webpage. We welcome feedback addressed to frmale@utexas.edu

1 **Comparison of permeability predictions on cemented**
2 **sandstones with physics-based and machine learning**
3 **approaches**

4 Frank Male*¹, Jerry L. Jensen², Larry W. Lake¹

5 1. Hildebrand Department of Petroleum and Geosystems Engineering, University of Texas
6 at Austin 2. Bureau of Economic Geology, University of Texas at Austin.

7 * frmale@utexas.edu

8 **Abstract**

9 Permeability prediction has been an important problem since the time of Darcy. Most
10 approaches to solve this problem have used either idealized physical models or empirical
11 relations. In recent years, machine learning (ML) has led to more accurate and robust, but
12 less interpretable empirical models. Using 211 core samples collected from 12 wells in the
13 Garn Sandstone from the North Sea, we compared idealized physical models based on the
14 Carman-Kozeny equation to interpretable ML models. We found that ML models trained on
15 estimates of physical properties are more accurate than physical models. Also, we found
16 evidence of a threshold of about 10% volume fraction, above which pore-filling cement
17 strongly affects permeability.

18 **Introduction**

19 Sandstone is one of the most common types of reservoir rocks, contributing approximately
20 30% to the stratigraphic total of sedimentary rocks (Pettijohn, 1975). It is the lithology for
21 eight of the ten largest gas fields in the world (Walsh and Lake, 2003; Sandrea, 2005).

22 Therefore, it is of interest to predict the reservoir properties of sandstones. This paper will
23 focus on analyzing the factors that influence sandstone permeability.

24 At least two broad approaches are available for permeability prediction of sandstones: 1)
25 physics-based models, such as the Carman-Kozeny equation and its derivatives, and 2)
26 empirical models, developed using statistical or machine learning (ML) tools that assume
27 no particular physical laws linking predictors and permeability. There are several physics-
28 based and empirical models; Dullien (2012) gives a good review of both model types. We
29 will apply a hybrid approach that considers both the physical intuition encapsulated in the
30 Carman-Kozeny equation and data-centric models. The novelty of our work is that it
31 compares the results of the physics-only and physics plus data driven models.

32 Kozeny (1927) and Carman (1937) developed an equation linking permeability to three
33 factors: porosity, hydraulic tortuosity, and specific surface area. Porosity and permeability
34 are routinely measured during core analysis, but hydraulic tortuosity (as opposed to
35 electrical tortuosity) and specific surface area are rarely evaluated although some log-
36 derived quantities are surrogates for this. However, both tortuosity and specific surface
37 area arise from geologic processes that can be modeled and distributed throughout the
38 reservoir. Therefore, understanding the magnitude and effect of tortuosity and surface area

39 can aid in building accurate permeability predictors and applying these predictions in
40 geomodels.

41 Panda and Lake (1995) developed a mathematical framework for estimating tortuosity and
42 specific surface area for real rocks that had undergone diagenesis. The framework, can
43 predict permeability from the intergranular porosity, the average grain diameter, the grain
44 size distribution, and the amounts and types of various cements.

45 Machine learning can be used to understand how useful tortuosity and specific surface area
46 are for predicting permeability. With advanced non-parametric ML (such as the gradient
47 boosting machine developed by Friedman, 2001), there is no requirement to assume *a*
48 *priori* a functional form between these variables and the predicted quantity. With the
49 recent derivation of a consistent feature attribution system for explaining tree-based
50 models (Lundberg et al., 2018), the functional form can be visualized after modeling; this
51 may help petrophysicists to understand the mechanisms controlling permeability.

52 In this study, we develop estimates for the permeability of the Garn Sandstone reservoir
53 (Ehrenberg, 1990), using the data from the 12 wells in that study. The Garn is a Middle
54 Jurassic formation in the North Sea, in the Haltenbanken area (Ehrenberg, 1990) that was
55 deposited in fluvial and near-shore marine environments (Gjelberg et al., 1987). It is
56 composed mostly of quartz grains and secondarily with feldspar (Ehrenberg, 1990). We
57 compare different methods for calculating the tortuosity and specific surface area from
58 core description, and we find the most important determinants of permeability predictors
59 for this data. Our analysis shows that porosity best predicts permeability, followed by the
60 presence of pore bridging cement and then tortuosity. Given the physics-based model and

61 advanced ML estimators, we propose a hybrid approach, combining the best qualities of
62 each method.

63 **Methods**

64 *Physical models*

65 Perhaps the best-known physics-based relationship to estimate permeability was
66 developed by Kozeny (1927) and later modified by Carman (1937). In its modern form, the
67 equation is written as

$$68 \quad k = \frac{\phi^3}{2\tau(1 - \phi)^2 a^2},$$

69 which, for simplicity, we will write as

$$70 \quad k = \frac{\phi_{CK}}{2\tau a^2},$$

71 where permeability is k , porosity is ϕ , tortuosity is τ , the specific surface area (wetted
72 area/volume) is a , and the Carman-Kozeny void fraction is ϕ_{CK} . For an uncemented
73 sandstone, tortuosity can be calculated following the derivation in Appendix A, which
74 comes from Panda and Lake (1994). For a cemented sandstone (Appendix B), the tortuosity
75 changes because of cements blocking and forcing modification of the flow paths.

76 For monodisperse spheres, $a = 6/d$, where d is the sphere diameter. For uncemented
77 spheres of more than one size, a can be estimated from the particle size distribution
78 (sorting) (Panda and Lake, 1994). After cementation, the cement distribution is a further

79 control on how the surface area changes. Some cements will coat the pores walls, slightly
80 decreasing the specific surface area. Other cements will line or bridge the pores,
81 moderately to greatly increasing the specific surface area.

82 A different model is based on the idea that pore throat sizes are an important variable in
83 permeability models. This hypothesis is implicit in the Winland-style relations that follow
84 the form

$$85 \quad \ln r = A \ln k - B \ln \phi + C$$

86 where r is the pore throat radius (see Kolodzie, 1980; Di and Jensen, 2015).

87 Doyen (1988) formalized this approach, applying effective medium theory to explain
88 permeability with the equation

89

$$90 \quad k = \frac{\phi r_{eff}^4}{8\tau \langle r_t^2 \rangle}$$

91 where r_{eff} is the effective pore throat radius and $\langle r_t^2 \rangle$ is the spatial average of the square of
92 the pore channel radii. This result is remarkably similar to the Carman-Kozeny equation,
93 except that the dependency on specific surface area has been replaced with a dependency
94 on the pore throat radii.

95 As a practical consideration, the pore throat radius might be more impacted by cements
96 that coat the walls than cements that bridge the pores. However, the opposite is true for the
97 specific surface area (Scheidegger, 1960).

98 *Data-driven models*

99 Empirical models have long been important in reservoir engineering (see Frick, 1962 for
100 numerous examples). These models, such as Winland's equation (Kolodzie, 1980), seek out
101 relationships between predictor variables (independent variables) and responses
102 (dependent variables – here, permeability). In the last two decades, advances in applied
103 statistics and computing power have created new approaches for developing empirical
104 relationships. This has spawned the field of data analytics and the attendant study of ML.

105 The data analytics approach is as follows:

- 106 1. collect and clean data
- 107 2. propose physics-based predictor variables
- 108 3. perform exploratory analysis
- 109 4. build machine learning models on a subset of the data (training data)
- 110 5. evaluate the machine learning models on new data (testing data)
- 111 6. interpret model results.

112 We apply the above workflow to data from Ehrenberg (1990). We chose this dataset
113 because it has a large range of permeability and porosity, cement proportions are
114 measured, and it requires only minimal cleaning. However, lacks many of the variables in
115 the Carman-Kozeny equation. Therefore, we performed feature engineering to derive these
116 variables from Ehrenberg's measurements. Among the variables we did not have were the
117 mean particle size, the coefficient of variation of the particle size, and the skewness of the
118 particle size distribution. These variables were derived through the procedure given in
119 Appendix C.

120 During exploratory data analysis, we plot the distributions of predictor and response
121 variables and make cross-plots between variable pairs to identify predictor variables with
122 strong co-linearity and with strong correlation to the response variable. For the Garn
123 sandstone, the predictor variables include the porosity, the Carman-Kozeny void fraction,
124 the Carman-Kozeny predictions of permeability, and the volume fractions of pore-filling
125 and pore-bridging cement present.

126 Ehrenberg (1990) estimated porosity two ways: Helium porosimetry, and point counting
127 the intergranular macroporosity of thin sections. These measurements are highly
128 correlated, so including both in the regression model could cause overfitting and
129 overestimate the influence of porosity on the permeability (feature importance would be
130 split between the two porosity measures). Therefore, we chose to use a single porosity
131 estimate. Exploratory data analysis showed that intergranular macroporosity was a better
132 predictor of permeability than Helium porosity, and we chose it for the model.

133 We used two approaches to build the models: multiple linear regression and gradient
134 boosting regression (Friedman, 2001). Multiple linear regressions are common, easily
135 interpretable, and robust to overfitting. These regressions also make several assumptions
136 that are often violated in real data sets, including a linear model relating predictors and
137 response variables, Gaussian distributions, and homoscedastic residuals. Gradient boosting
138 regressors make fewer assumptions about the distributions of the input data and the
139 character of the relationship between predictor variables and the response, but their
140 results are difficult to interpret and prone to overfitting. To illustrate the benefits and
141 drawbacks of these approaches, we use both methods and compare the results.

142 Through careful feature selection and pre-processing, we limited the degree to which the
143 assumptions in linear regression are violated. As aforementioned, one of those steps is
144 removing highly correlated predictor variables. In addition, we log-transformed the
145 predictor variables and permeability, which reduces non-normality of the variables'
146 distributions. Log-transformation also makes the correlations between variables more
147 linear. Using the Box-Cox (1964) transformation did not significantly improve the results,
148 but it can be effective in some cases, as shown by Jensen et al. (1987).)

149 We evaluated the models through calculating the model explained variance (R^2), mean
150 absolute error (MAE), and root-mean squared error (RMSE). The equations for these
151 measures are as follows

152

$$R = \frac{1}{n-1} \sum_i^n \frac{y_i - \bar{y}}{\sigma_y} \frac{y'_i - \bar{y}'}{\sigma_{y'}}$$

153

$$\text{RMSE} = \left(\frac{1}{n} \sum_i^n (y_i - y'_i)^2 \right)^{1/2}$$

$$\text{MAE} = \frac{1}{n} \sum_i^n |y_i - y'_i|$$

154 where n is the sample size i represents the sample number, y is the actual value, y' is the
155 predicted value, a bar over a quantity is the sample mean of that quantity, and σ is the
156 sample standard deviation of a quantity.

157 Hyperparameters for the gradient boosting regressor were selected through cross-
158 validation. During cross-validation, candidate models are fed data on seven of the eight
159 wells in the training data, then scored based on which minimizes the RMSE predicting the

160 excluded well. This is iterated through each well and a gamut of hyperparameters. Through
161 this procedure, we maximize the model effectiveness while reducing overfitting by
162 minimizing the validation RMSE on held-out data (four wells in the testing data).

163 In order to determine whether predictor variables contributed to the result, we used a non-
164 parametric approach. This approach is called Permutation Feature Importance (Fisher, et
165 al., 2018), and estimates the importance of a predictor variable based on how much the
166 model error increases after that variable is permuted (randomly shuffled).

167 Linear models can be interpreted simply through examining the weight assigned to each
168 predictor (feature). Gradient boosting methods require a different approach. SHapley
169 Additive exPlanations (SHAP values) offer a way to explain how each predictor variable
170 contributed to each prediction (Lundberg and Lee, 2016). The idea behind Shapley values
171 is to determine how much each input affects the output for each individual prediction. To
172 do this, SHAP values use an idea borrowed from cooperative game theory (Shapley, 1953),
173 where the actors work together as a team to achieve a result, leading to a pay-out
174 proportional to how much each actor contributed to the final result. We use an exact
175 solution for SHAP values (Lundberg and Lee, 2016) that has been implemented in the
176 XGBoost library (Chen and Guestrin, 2016).

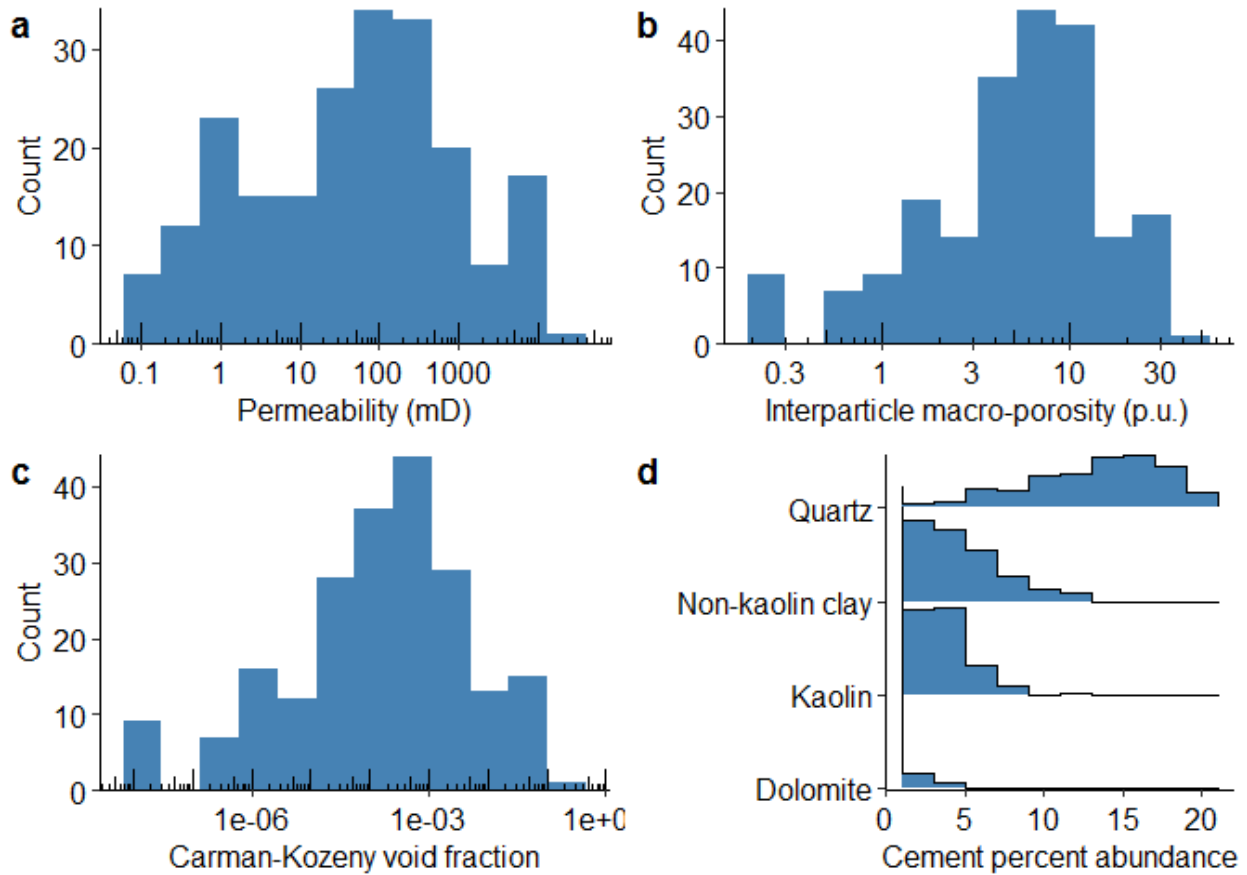
177 **Results**

178 *Exploratory analysis*

179 First, we examined the distributions for porosity, permeability, Carman-Kozeny void
180 fraction, and the proportion of various cements (Fig. 1). The permeability, porosity—and
181 therefore Carman-Kozeny void fraction—distributions follow a bi-modal distribution. The
182 permeability histogram is the most clearly bi-modal (modes of approximately 0.8 and 90
183 md) of the three parameters, but a minor mode also exists in the porosity histograms
184 ($\log\phi$ modes at approximately 1.8 and 6 pu). Multimodal distributions are common in
185 subsurface data and can be indicative of multiple facies (Jensen et al., 2000). An
186 appropriate treatment of bi-modal data is to analyze each mode separately, splitting the
187 analysis into high porosity and low porosity assessments.

188 Therefore, when we performed regressions on the data, we treated each mode separately,
189 rather than regressing across the entirety of the data. The data was split into two classes:
190 samples where the interparticle macro-porosity is greater than 2.3% (high) or less than or
191 equal to 2.3% (low). The cutoff was selected through using Gaussian Mixture Modeling
192 (Fraley and Raftery, 2002) to separate the modes..

193 There are 163 points in the high porosity training set, 41 points in the high porosity testing
194 set, 48 points in the low porosity training set, and 20 points in the low porosity testing set.

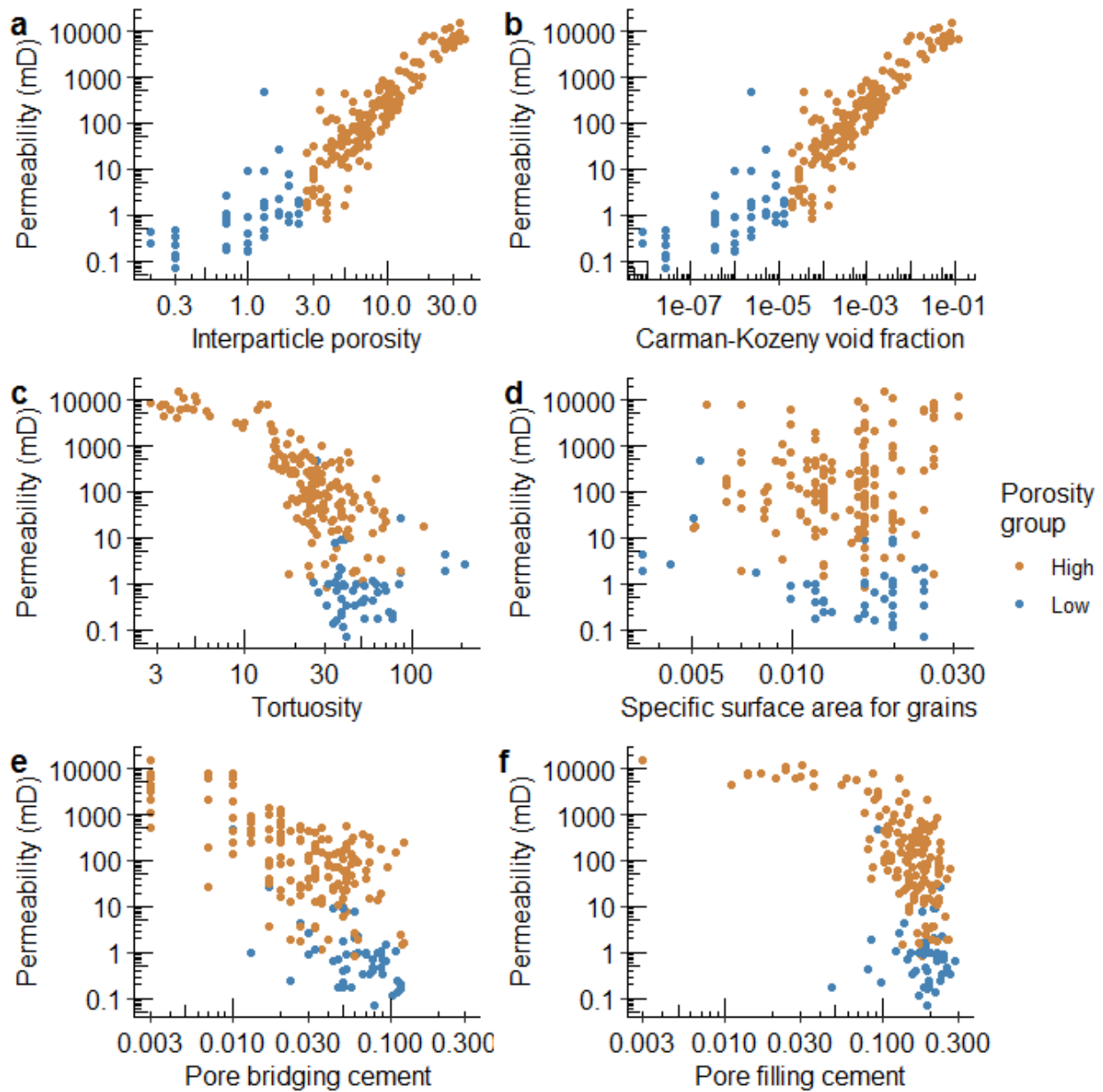


195

196 Figure 1. Histograms for the distributions of a) Klinkenberg-corrected absolute
 197 permeability b) interparticle macro-porosity from point-counting c) Carman-Kozeny void
 198 fraction from macro-porosity d) Percent abundances (total area fraction) of cement. The
 199 permeability and porosity, both log-transformed, follow bimodal distributions. Quartz is
 200 the most abundant cement, followed by non-kaolin clay (smectite and illite).

201 Next, we cross-plotted permeability against several individual predictors (Fig. 2): Carman-
 202 Kozeny void fraction, tortuosity, pre-cementation specific surface area, and fraction of
 203 pore-bridging and pore-filling cement. Pore-filling cement includes quartz, kaolin clay, and

204 dolomite, and pore-bridging cement is non-kaolin clay.



205

206 Figure 2. Cross-plots between permeability and several predictor variables. These variables

207 include a) the interparticle macro-porosity b) the Carman-Kozeny void fraction, c)

208 tortuosity as calculated in Panda and Lake (1995), d) specific surface area in reciprocal

209 square microns for the grains (pre-cementation), e) fraction of pore-bridging cement f)

210 fraction of pore-filling cement. The color indicates whether the sample has greater than 2.3
 211 percent porosity (orange) or not (blue).

212 To assign values to the correspondence between the predictor variables and permeability,
 213 we calculated the Pearson's r and Kendall tau values (Table 1). Both statistics measure the
 214 degree of association between the variables and have values between -1 and 1. Pearson's
 215 statistic is a measure of linear correlation and based on the data values; Kendall's statistic
 216 is based on the ranks of the data values. More details can be found in many statistics texts,
 217 including Miller (1986).

218 Table 1. Pearson r and Kendall tau values for correlation between log-transformed
 219 predictor variables and log permeability. The data is split between modes of the porosity
 220 distribution, based on whether or not the porosity is greater than 2.3. Tortuosity is
 221 calculated after taking cementation into account; specific surface area is calculated without
 222 including cementation – making the presence of pore-bridging and pore-filling cements
 223 into proxies for specific surface area.

Porosity group	Correlation	Carman-Kozeny void fraction	Tortuosity	Specific surface area	Pore-bridging cement	Pore-filling cement
High	Pearson r	0.90	-0.77	0.18	-0.71	-0.63
High	Kendall tau	0.73	-0.57	0.11	-0.46	-0.40
Low	Pearson r	0.48	0.06	-0.42	-0.59	-0.09
Low	Kendall tau	0.44	0.02	-0.15	-0.31	-0.06

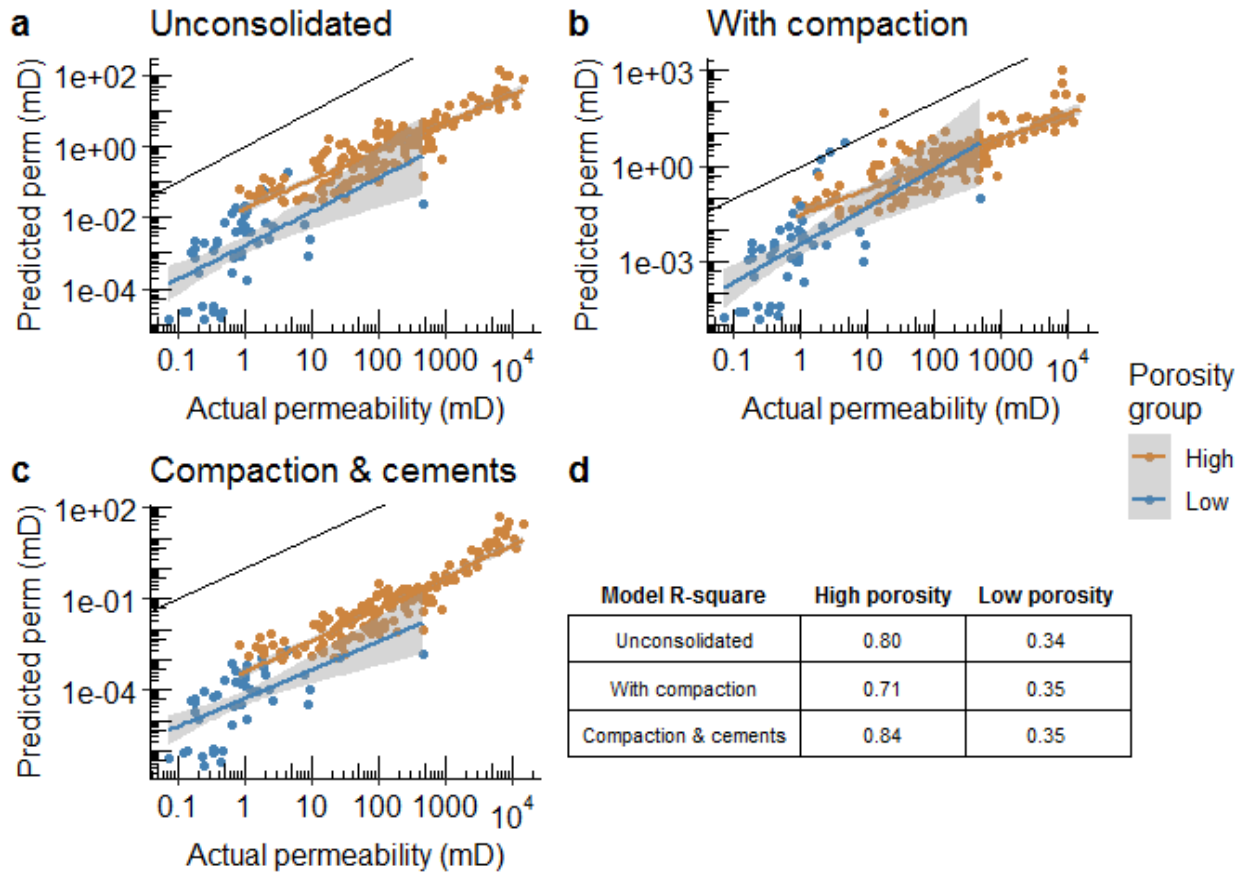
224 The two correlation measures show similar values within each porosity group, however
225 they take on different values between the porosity groups, with less correlation at low
226 porosity. Porosity is the most strongly correlated with permeability, with cements next,
227 and tortuosity and specific surface area having the weakest correlations.

228 *Model results*

229 We tested the accuracies and correlations between the physics-based and regression-based
230 models and the measured permeability. The three physics-based models of increasing
231 complexity are:

- 232 1. Classic Carman-Kozeny model with no compaction or cementation effects
- 233 2. Carman-Kozeny model with the effect of compaction on the grain size distribution
- 234 3. Carman-Kozeny including compaction and cement's effect on tortuosity

235 The results from these models of increasing complexity are shown in Fig. 3.



236

237 Figure 3. Comparisons of physics-based models to measured permeability. The black line
 238 indicates perfect agreement. The colored lines are least-squares best fits. Shading indicates
 239 95% uncertainty in the best fit line. a) Uses the Carman-Kozeny void fraction and the initial
 240 tortuosity and specific surface area expected from an uncompacted particle assemblage of
 241 the measured porosity and grain size. b) Considers compaction with the Panda-Lake
 242 (1994) model. c) Considers the impact of compaction and the effect of cementation on the
 243 tortuosity, following the Panda-Lake (1995) model. d) R² for the log-permeability predicted
 244 by these models compared to observed in the core.

245 Including compaction and cementation modestly improves the Carman-Kozeny model R²
 246 by 0.05 for the high porosity sandstone, but weakly for low porosity samples (Fig 3d). High

247 porosity samples are better predicted than low porosity samples. All sample permeabilities
248 are significantly underpredicted by approximately two to three orders of magnitude by the
249 physics-based models, which have no fitting parameters.

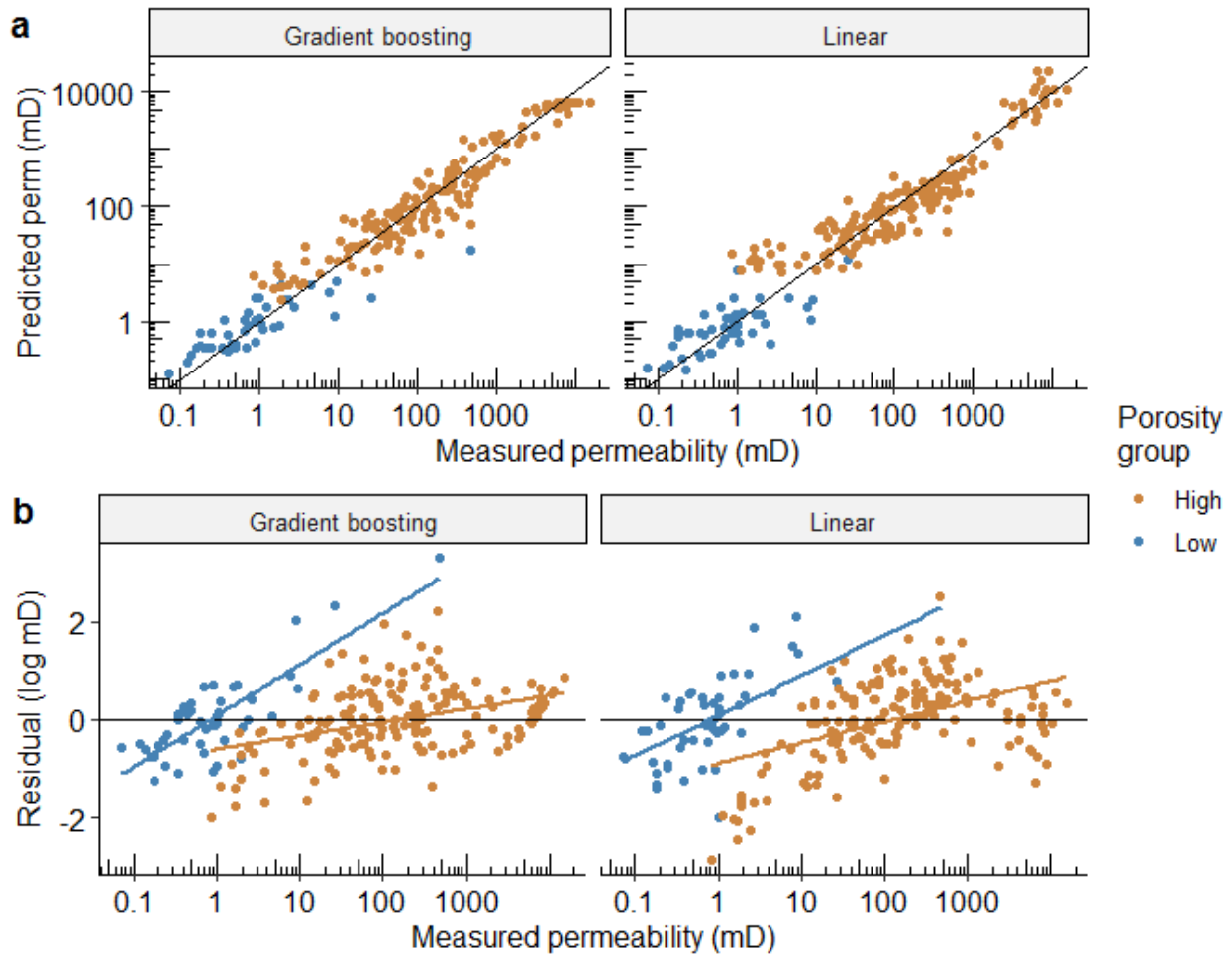
250 In addition to the three physics-based models, we tested two physics-inspired, regression-
251 based models (Fig. 4):

252 4. A linear model using a Winland-style equation of the form

253
$$\ln k \propto \ln \phi_{CK} + \ln a_u + \ln \tau_e + \ln P_b + \ln P_f,$$

254

255 5. A gradient boosting model using the same predictor variables, but assuming no
256 particular functional form between the variables and permeability



257

258 Figure 4. a) Predicted versus measured permeability using the linear and gradient boosting

259 models. b) Residuals in the predictions for the linear and gradient boosting models. Color

260 indicates whether the sample is in the high (greater than 2.3%) or low porosity group.

261 Lines indicate the trends in the residual.

262 The XGBoost hyperparameters that best match permeability for low porosity rock are 520

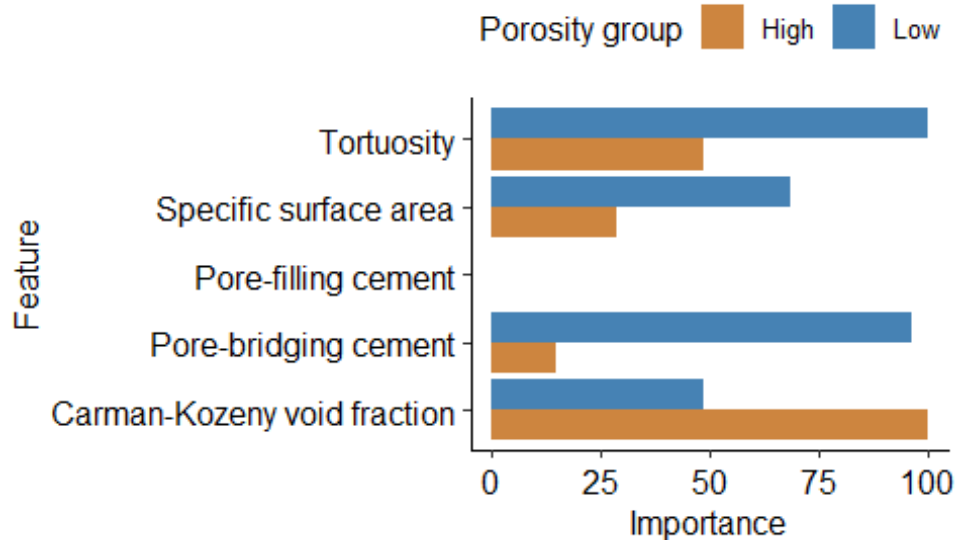
263 trees, a learning rate of 0.02, no minimum loss reduction (γ), a max tree depth of 1,

264 0.78 of the columns sampled by each tree, and a minimum child weight of 7 samples. For

265 the high porosity rock, they were 550 trees, a learning rate of 0.017, a maximum tree depth

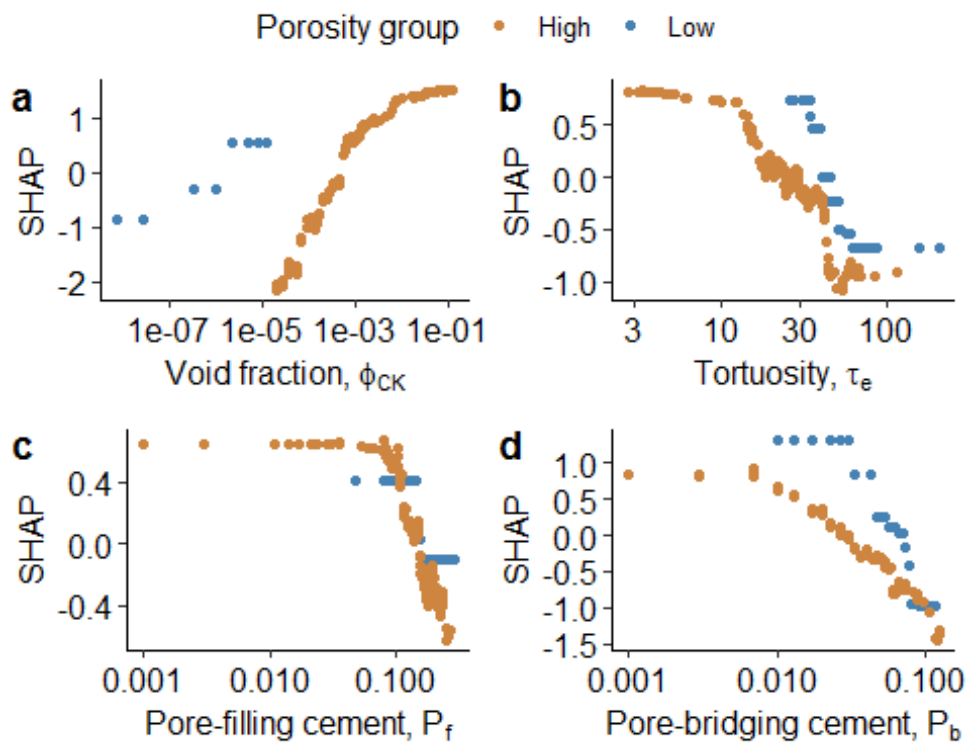
266 of 2, a minimum loss reduction of 0.94, 0.69 of the columns sampled by each tree, a
267 minimum child weight of 2, and a subsample ratio of 0.23 for the training instances.
268 The linear model Elastic net hyperparameters that best match permeability for low
269 porosity samples cause no regularization. For high porosity samples, the hyperparameters
270 are a regularization constant of 0.15 and an alpha of 0.02, indicating primarily ridge style
271 regression.

272 As perhaps best shown by the residuals and best fit lines (Fig. 4b), neither model is
273 explaining all the permeability variation with the chosen predictors and models. That is to
274 say, there is a functional relationship between the residual values of the prediction and the
275 value of the permeability. Fig. 4a gradient boosting shows no predictions above 5220 md, a
276 result of the minimum number of points allowed in each split of the gradient boosting
277 trees. Fig. 4b shows that residuals follow a quadratic function at high porosity, indicating a
278 higher-order (than linear) relationship between one or more of the predictors and
279 permeability.



281 Figure 5. Feature importance for the linear model. Color indicates whether the model was
282 trained on high (greater than 2.3%) or low porosity samples. No bar indicates that the
283 regularization procedure caused the weight for that feature to reach zero.

284 The linear model shows different features are important for high versus low porosity
285 samples (Fig. 5). Carman-Kozeny void fraction is the most important factor for high
286 porosity rock, followed by tortuosity and specific surface area. For low porosity samples,
287 tortuosity and the fraction of pore-bridging cement are the most important features. In
288 neither group is the fraction of pore-filling cement an important feature, both models
289 assign it zero weight (i.e., it does not directly influence permeability).



290

291 Figure 6 . Feature importance for the gradient boosting model, using SHapely Additive
292 exPlanations (SHAP). SHAP values use game theory to explain how much each element

293 contributes to each prediction from the gradient boosting model. Orange dots show high
 294 porosity samples, while blue samples indicate low porosity samples. The SHAP values are
 295 for the following features: a) Carman-Kozeny void fraction b) Tortuosity c) volume fraction
 296 of pore-filling cement d) volume fraction of pore-bridging cement.

297 For the gradient boosting model (Fig. 6), each dot represents the importance for a
 298 particular sample. A zero SHAP value indicates no influence of the chosen predictor on the
 299 permeability for that sample. The largest influence on permeability comes from void
 300 fraction for high porosity samples, and the fraction of pore-bridging cement for the low
 301 porosity samples. Tortuosity and the fraction of pore-filling cement are of secondary
 302 importance, and the specific surface area (before cementation) is least important.

303 The SHAP values for pore filling cement concentration follow a sharply sigmoidal shape,
 304 implying a transition point around 10% cementation. Other features show more samples in
 305 their linear trend, with the effects of extreme points leveling off because of limited data.

306 Table 2. Measures of model fitness for the gradient boosting and linear models on the high
 307 porosity and low porosity groups for the training and testing data.

Model	Porosity group	Data	RMSE	MAE	R ²
Gradient boosting	Low	Train	0.85	0.59	0.74
Gradient boosting	Low	Test	1.31	1.07	0.52
Gradient boosting	High	Train	0.71	0.55	0.90
Gradient boosting	High	Test	0.97	0.72	0.83

Linear	Low	Train	0.85	0.68	0.69
Linear	Low	Test	1.74	1.35	0.49
Linear	High	Train	1.64	1.33	0.69
Linear	High	Test	1.73	1.37	0.67

308 The model metrics (Table 2) indicate that the gradient boosting method leads to smaller
309 residuals and a higher R^2 than the linear model. For most cases, the models work better on
310 cross-validation training data than testing data. For comparison, a porosity-only log-linear
311 model has $R^2=0.81$ for high porosity, 0.23 for low porosity. The gradient boosting model
312 has better explanatory value than porosity alone, while the linear model has roughly the
313 same explanatory value. Both models outperform the porosity-only model at low porosity.
314 They also significantly outperform the physics-based models at low porosity.

315 Discussion

316 We have presented several methods for estimating permeability from thin section data for
317 sandstone samples. First, we used several physics-based models of increasing complexity.
318 Then, we built hybrid data-driven models with physical parameters as inputs. The data-
319 driven models performed better than the purely physics-based models.

320 A key step in this analysis is splitting the data into two parts, each containing one mode of
321 porosity. Why have we done this? During exploratory analysis, we saw that the
322 permeability distribution was bi-modal, and the porosity distribution did not match either
323 a normal or a log-normal distribution. Multi-modal permeability distributions are a

324 common problem in permeability modeling (see, *e.g.* Clarke, 1979; Dutton and Willis, 1998;
325 and Jensen et al., 2000). One approach for treating multiple modes is to split the
326 distribution by mode and analyze each separately. This approach is particularly useful for
327 reservoirs, where identifying the causes for high permeability zones is important, and the
328 magnitude of low permeability zones may be less important. The splits can be selected
329 through visual inspection, Gaussian Mixture Models (Fraley and Raftery, 2002), or k-means
330 clustering (Likas et al., 2003).

331 The next step of the exploratory analysis is summarized in Table 1. Consistent with many
332 other studies (*e.g.*, Amyx et al., 1960; Slatt, 2006; Doveton, 2014; Baker et al., 2015), we see
333 that porosity has a strong correlation with permeability for the larger-porosity data. There
334 is, however, little to no correlation for low permeability rock, similar to patterns observed
335 elsewhere (*e.g.*, Broger et al., 1997, their Fig. 10; Wendt et al., 1986, their Figs. 2 and 7). In
336 fact, no single parameter correlates strongly with permeability for the low-porosity
337 samples. The Pearson and Kendall correlations are informative, but determining true
338 feature importances requires interrogating a regression model.

339 Physics-based models based on successively more complex modifications of the Carman-
340 Kozeny equation were tested on the data. We found that including the effect of compaction
341 on the flow properties was not sufficient to improve the model without including
342 cementation. This is in contrast to the findings of Panda and Lake (1994), but consistent
343 with their later work (Panda and Lake, 1995), which included cementation.

344 Two ML-based models were trained and tested on the data. The Winland-style linear model
345 was the less accurate of the two, but it still provided insights into the relative importance of

346 different physical effects on permeability. The gradient boosting model was more accurate
347 overall and showed a nonlinear effect coming from cementation. However, in a relatively
348 low data environment it loses some resolution in the predictions at the extremes of high
349 and low permeability (see Fig 4a, the top 10 permeability points). The benefits of using the
350 linear model were 1) The model is relatively simple with few parameters to evaluate; 2) the
351 permeabilities above 5000 md were better predicted than with the gradient boosting
352 model. The gradient boosting model, however, could be used with SHAP evaluations to
353 identify control strengths for each sample. This option could be quite useful in other cases
354 if geological information were also available. For example, one might look for changes in
355 the strengths of the predictor variables according to the facies from which the sample was
356 taken.

357 All of the models tested performed worse at predicting permeability at low porosity. This is
358 likely because of the higher tortuosity and specific surface areas, more cementation, and
359 smaller pore throats at this porosity range. Alternatively, we might have failed to measure
360 an important permeability predictor.

361 There has been healthy debate on whether Doyen's (1988) pore throat size based approach
362 or Panda and Lake's (1995) specific surface area approach tell us more about the
363 permeability of sandstones. After building and interpreting two machine learning models,
364 this study can now shed some light on the question.

365 The feature importances from the logarithmic regression provide evidence that pore throat
366 size is more important than specific surface area in determining permeability. On the other

367 hand, the degree of pore-filling cement present is not important. This recommends
368 measuring pore throat sizes over determining specific surface area.

369 From the gradient boosting model, we see that specific surface area is less important than
370 void fraction, tortuosity, and the degree of cementation. However, this measure of specific
371 surface area does not include the cementation effect because Panda and Lake did not
372 provide values for calculating surface area from the amount of pore-filling and pore-
373 bridging cement. We see from the SHAP values (Figure 6) that this could be a strong effect
374 following a sigmoidal functional form.

375 The SHAP values for pore-filling and pore-bridging cement indicate that pore-bridging
376 cement is more important for determining permeability, which is consistent with either a
377 surface area or pore throat-centric paradigm. However, for all cements, there appears to be
378 a threshold around 10% volume fraction, after which permeability drops drastically. This
379 could indicate that, while specific surface area and pore throat radius are both good
380 explanatory variables for interpreting permeability, at around 10% cementation, pores and
381 pore throats are blocked, and this is the dominant effect on permeability. From another
382 perspective, 10% cements could be interpreted as a percolation threshold. This value is
383 less than the threshold values suggested by Korvin (1992) (0.25 to 0.5) but within the
384 range of values calculated by Deutsch (1989) (0.1 to 0.5).

385 **Conclusions**

386 We used a sandstone dataset to test several models for predicting permeability in the
387 presence of cementation. We found the following:

- 388 1. Machine learning provides better data correlation than even advanced Carman-
389 Kozeny models.
- 390 2. Gradient boosting can improve upon linearized regression, and helps to identify
391 nonlinear effects coming from cementation.
- 392 3. As a first step analysis, porosity is a remarkably good predictor of permeability at
393 porosities greater than 2.3 %, after it has been transformed to Carman-Kozeny void
394 fraction.
- 395 4. To improve upon porosity-only predictions in sandstones using thin section analysis,
396 pore-bridging cement amounts should also be evaluated.
- 397 5. For the Garn sandstone, the importance of variables is as follows:
- 398 – High porosity: porosity, cements, tortuosity, and specific surface
- 399 – Low porosity: pore-bridging cement, porosity, tortuosity, pore-filling cement

400 **Acknowledgements**

401 We are grateful to Stephen Ehrenbreg for the kind donation of his core analysis of the Garn
402 formation. We thank Ian Duncan and William Abrose for valuable discussions during the
403 preparation of this manuscript and Behzad Ghanbarian for suggestions regarding
404 theoretical calculations of tortuosity. This study was funded in part by the US Department
405 of Energy (DOE) grant FE0024375 (PI: Ian J. Duncan) and in part by the State of Texas
406 Advanced Resource Recovery Program (PI: William A. Ambrose). Statistical analysis was
407 performed in the R language (R Core Team, 2014). Plots were generated using the GGPlot2

408 package (Wickham, 2009). Larry W. Lake holds the Shahid and Sharon Chair at the
409 Hildebrand Department of Petroleum and Geosystems Engineering.

410 **References**

411 Amyx, J. W., Bass, D. M., and Whiting, R. L., 1960, *Petroleum Reservoir Engineering*, McGraw-
412 Hill.

413 Baker, R. O., Yarranton, H. W., and Jensen, J. L., 2015, *Practical Reservoir Engineering and*
414 *Reservoir Characterization*, Gulf Prof. Pub.

415 Beard, D.C. and Weyl, P.K., 1973. Influence of texture on porosity and permeability of
416 unconsolidated sand. AAPG Bulletin, 57(2), pp.349-369.

417 Box, G. E. P., Cox, D.R., 1964. An analysis of transformation revisited, rebutted, Journal of
418 the American Statistical Association, 77, pp. 209-210.

419 Broger, E. J. K., Syhlonyk, G. E., and Zaitlin, B. A., 1997. Glauconite Sandstone exploration: A
420 case study from the Lake Newell Project, southern Alberta. In *Petroleum Geology of the*
421 *Cretaceous Mannville Group, Western Canada*, S. G. Pemberton and D. P. James (eds.), CSPG
422 Memoir 18, pp 140-168.

423 Carman, P.C., 1937. Fluid flow through granular beds. Trans. Inst. Chem. Eng., 15, pp.150-
424 166.

425 Chen, T. and Guestrin, C., 2016, August. Xgboost: A scalable tree boosting system. In
426 *Proceedings of the 22nd ACM SIGKDD international conference on knowledge discovery and*
427 *data mining* (pp. 785-794).

428 Comisky, J. T., Newsham, K. E., Rushing, J. A., and Blasingame, T. A., 2007. A comparative

429 study of capillary-pressure-based empirical models for estimating absolute permeability in
430 tight gas sands. SPE conference paper SPE 110050 presented at the SPE Ann. Tech. Conf.
431 and Exhib., Anaheim CA 11-14 Nov., 18p.

432 Clarke, R.H., 1979. Reservoir properties of conglomerates and conglomeratic sandstones.
433 AAPG Bulletin, 63(5), pp.799-803.

434 Di, J. and Jensen, J.L., 2015. A closer look at pore throat size estimators for tight gas
435 formations. Journal of Natural Gas Science and Engineering, 27, pp.1252-1260.

436 Deutsch, C., 1989, Calculating effective absolute permeability in sandstone/shale
437 sequences. SPE Form. Eval., vol. 4(3), pp343-348.

438 Doveton, J. H., 2014, *Principles of Mathematical Petrophysics*, Oxford University Press.

439 Doyen, P.M., 1988. Permeability, conductivity, and pore geometry of sandstone. Journal of
440 Geophysical Research: Solid Earth, 93(B7), pp.7729-7740.

441 Dullien, F.A., 2012. *Porous media: fluid transport and pore structure*. Academic press.

442 Dutton, S.P. and Willis, B.J., 1998. Comparison of outcrop and subsurface sandstone
443 permeability distribution, lower Cretaceous fall river formation, South Dakota and
444 Wyoming. Journal of Sedimentary Research, 68(5), pp.890-900.

445 Ehrenberg, S.N., 1990. Relationship between diagenesis and reservoir quality in sandstones
446 of the Garn formation, Haltenbanken, mid-Norwegian Continental shelf (1). AAPG bulletin,
447 74(10), pp.1538-1558.

448 Fisher, A., Rudin, C. and Dominici, F., 2018. Model class reliance: Variable importance
449 measures for any machine learning model class, from the “Rashomon” perspective. arXiv
450 preprint arXiv:1801.01489.

451 Fraley, C., and Raftery, A.E., 2002. Model-based clustering, discriminant analysis and

452 density estimation, *Journal of the American Statistical Association*, 97(458), pp. 611-631.

453 Frick, T.C., 1962. *Petroleum production handbook* (Vol. 1). McGraw-Hill.

454 Friedman, J.H., 2001. Greedy function approximation: a gradient boosting machine. *Annals*
455 *of statistics*, pp.1189-1232.

456 Ghanbarian, B., Hunt, A.G., Ewing, R.P. and Sahimi, M., 2013. Tortuosity in porous media: a
457 critical review. *Soil science society of America journal*, 77(5), pp.1461-1477. Gjelberg J.,
458 Dreyer, T., Hoie, A., Tjelland, T., and Lilleng, T., 1987. Late Triassic to Mid-Jurassic sand
459 body development on the Barents and Mid-Norwegian shelf, in J. Brooks and K. Glennie,
460 eds., *Petroleum geology of north west Europe, London, Graham and Trotman*, p. 1105-1129.

461 Jensen, J. L., Hinkley, D. V., and Lake, L. W., 1987. A statistical study of reservoir
462 permeability: Distributions, correlations, and averages. *SPEFE*, 2(6), pp. 461-468.

463 Jensen, J.L., Lake, L.W., Corbett, P.W.M., and Goggin, D.J., 2000. *Statistics for petroleum*
464 *engineers and geoscientists*, 2nd ed. Elsevier, Amsterdam, 138 p.

465 Kolodzie Jr, S., 1980. Analysis of pore throat size and use of the Waxman-Smits equation to
466 determine OOIP in Spindle Field, Colorado. Paper SPE 9382 in 55th SPE annual technical
467 conference and exhibition. Society of Petroleum Engineers, 10p.

468 Korvin, G., 1992. *Fractal Models in the Earth Sciences*. Elsevier, Amsterdam.

469 Kozeny, J., 1927. Soil permeability. *Sitzungsber. Oesterr. Akad. Wiss. Wien. Math.*
470 *Naturwiss. Kl. Abt*, 136, p.271.

471 Likas, A., Vlassis, N. and Verbeek, J.J., 2003. The global k-means clustering algorithm.
472 *Pattern recognition*, 36(2), pp.451-461. Lundberg, S.M., Erion, G.G. and Lee, S.I., 2018.
473 Consistent individualized feature attribution for tree ensembles. arXiv preprint
474 arXiv:1802.03888.

475 Miller, R. G., 1986, *Beyond ANOVA, Basics of Applied Statistics*, J. Wiley and Sons, New York,
476 317p.

477 Ngo, V. T., Lu, V. D., Nguyen, M. H., Hoang, H. M., Le, V. M., and Son, L., 2015. A comparison of
478 permeability prediction methods using core analysis data. SPE conference paper SPE
479 175650 presented at the SPE Reservoir Characterization and Simulation Conf. and Exhib.,
480 Abu Dhabi, UAE 14-16 Sept. 16p.

481 Panda, M.N. and Lake, L.W., 1994. Estimation of single-phase permeability from parameters
482 of particle-size distribution. *AAPG Bulletin*, 78(7), pp.1028-1039.

483 Panda, M.N. and Lake, L.W., 1995. A physical model of cementation and its effects on single-
484 phase permeability. *AAPG Bulletin*, 79(3), pp.431-443.

485 Pettijohn, F. J., 1975, *Sedimentary Rocks*, Third Ed., Harper and Row, New York, 628p.

486 R Core Team, 2017. R: A language and environment for statistical computing. R Foundation
487 for Statistical Computing, Vienna, Austria. URL <http://www.R-project.org/>

488 Sandrea, R., 2005, Global natural gas reserves – a heuristic viewpoint. *Ipc66.com*, archived
489 4 March 2016. Scheidegger, A.E., 1960, *The Physics of Flow Through Porous Media*, Revised
490 Ed., University of Toronto Press.

491 Shapley, Lloyd S., 1953. A value for n-person games. *Contributions to the Theory of Games*
492 2(28), pp. 307-317.

493 Slatt, R. M., 2006. *Stratigraphic Reservoir Characterization for Petroleum Geologists,*
494 *Geophysicists, and Engineers*. Elsevier.

495 Thomas, S., Corbett, P. and Jensen, J., 1996, January. Permeability and Permeability
496 Anisotropy Characterisation in the Near Wellbore: A Numerical Model Using the Probe
497 Permeameter and Micro-Resistivity Image Data. In *SPWLA 37th Annual Logging Symposium*.

498 Society of Petrophysicists and Well-Log Analysts.
499 Walsh, M.P. and Lake, L.W., 2003. *A generalized approach to primary hydrocarbon recovery*
500 (Vol. 4). Amsterdam: Elsevier. p. 36.
501 Wendt, W. A., Sakurai, S., and Nelson, P. H., 1986. Permeability prediction from well logs
502 using multiple regression. In *Reservoir Characterization*, L. W. Lake and H. B. Carroll (eds.),
503 Academic Press, pp. 181-221.
504 Wickham, H. (2009) *ggplot2: elegant graphics for data analysis*. Springer New York.

505 **Appendix A. Derivation of a modified Carman-Kozeny equation for** 506 **uncemented sandstones**

507 This section follows the derivation laid out by Panda and Lake (1994).
508 The derivation starts with the Carman-Kozeny equation

$$509 \quad k = \frac{\phi^3}{2\tau(1 - \phi)^2 a^2},$$

510 where permeability is k , porosity is ϕ , tortuosity is τ , and the specific surface area is a . Both
511 the Helium porosity and the interparticle macroporosity have been measured on the Garn
512 data. Klinkenberg-permeability to air is also part of the dataset. To estimate tortuosity and
513 specific surface area, the dataset includes measurements of the median grain size and the
514 Trask sorting coefficient, following the approach proposed by Beard and Weyl (1973). The
515 skewness of the distribution of grain sizes can be extracted from these parameters.

516 Given this information, a modified Carman Kozeny equation following Panda and Lake
517 (1994) is

518
$$k = \frac{\bar{D}^2 \phi^3}{72\tau_u(1-\phi)^2} \frac{(\gamma C_D^3 + 3C_D^2 + 1)^2}{(1 + C_D^2)^2},$$

519 where \bar{D} is the mean particle size, C_D is the coefficient of variation of the particle size
520 distribution ($C_D = \sigma_D/\bar{D}$), γ is the skewness of the particle size distribution. and τ_u is the
521 tortuosity of an unconsolidated, uncemented sand.

522 Panda and Lake (1994) do not calculate the original tortuosity. However, there has been a
523 wealth of work on this problem in the physics, soil, and petroleum literature. One approach
524 is proposed by Ghanbarian, et al. (2013). This approach makes use of percolation theory
525 and results in tortuosity following a power law with respect to porosity. Taking their
526 equation 14 (which assumes monodisperse spheres at hexagonal close packing), original
527 tortuosity follows the equation

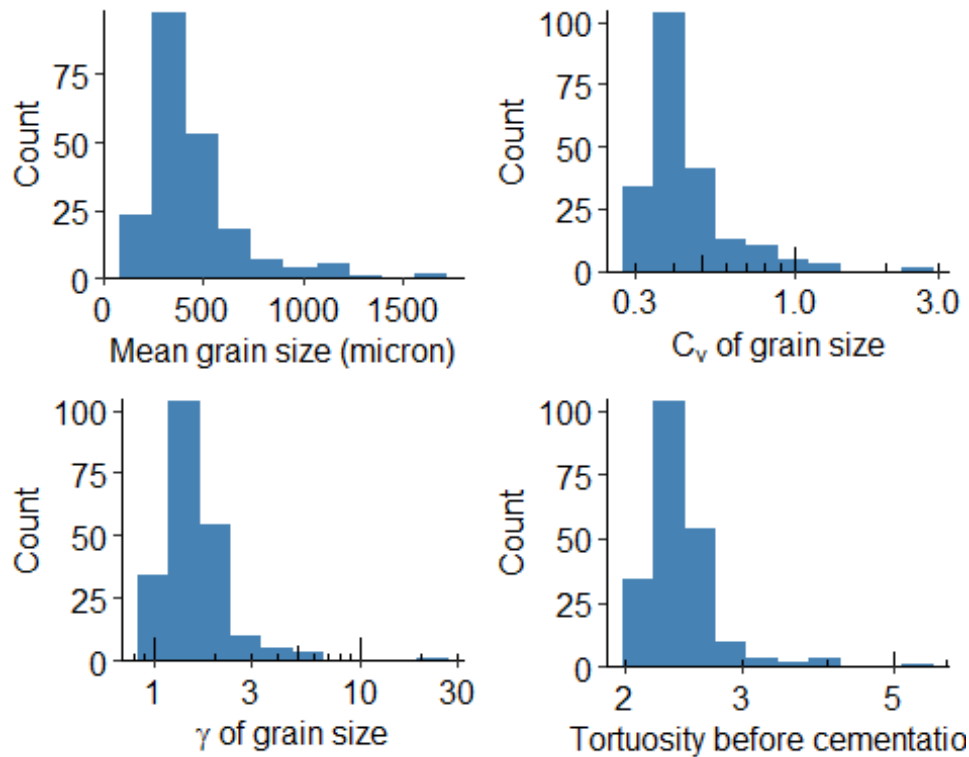
528
$$\tau_o = \sqrt{\frac{2\phi}{3[1 - B(1 - \phi)^{2/3}] + \frac{1}{3}}}$$

529 where $B = 1.209$.

530 Panda and Lake (1995) use a surface area argument to derive the effective tortuosity for an
531 uncemented sandstone of different size particles, which is

532
$$\tau_u = \tau_o(1 + C_D^2).$$

533 The distributions of the grain distribution measures, \bar{D} , C_D , γ , and the tortuosity τ_u are
534 given in Fig. A1. These measures are all highly skewed.



535

536 Figure A1. Histograms of several grain properties.

537 **Appendix B: Derivation of Carman-Kozeny corrections for cemented**
538 **sandstones**

539 This section follows the derivation laid out by Panda and Lake (1995).

540 Carman-Kozeny theory does not consider the effect of cementation on permeability, but
541 cement is present in these rocks, and it blocks flow paths, decreasing the rock permeability.

542 In terms of the quantities considered by Carman and Kozeny, this changes the tortuosity

543 and the specific surface area. There are several different cements that are present, and
544 they are measured through point counting.

545 Panda and Lake (1995) separate cement types into three categories: pore-filling, pore-
546 lining, and pore-bridging, following Neasham (1997). Where cements associate with the
547 pores depends on the thermodynamic properties of the cementing material. Crystal-like
548 kaolinite and dickite cements are pore-filling. Other pore-filling cements include quartz,
549 feldspar, dolomite, and calcite. These cements affect the porosity, but because they do not
550 affect the pore throats or the pore shape, under this model they have a small effect on
551 permeability.

552 Pore-lining cements find it energetically favorable to form long crystals that stretch out
553 from the grains. These cements include the non-kaolinite clay minerals, such as chlorite,
554 illite, and smectite. The long crystals affect permeability more than they affect porosity
555 because of the large surface areas they generate.

556 Pore-bridging cements can partially or completely block the pore throats, decreasing the
557 accessible porosity. This strongly influences the permeability through increasing the
558 tortuosity of the system and decreasing the connectivity. Examples of the minerals that
559 bridge pores include illite, chlorite, and montmorillonite (the non-Kaolin clay minerals).

560 After cementation, the tortuosity and specific surface area has changed. Panda and Lake
561 (1995) suggest an effective tortuosity, τ_e , given by

562
$$\tau_e = \tau_u(1 + C_D^2) \left(1 + \frac{Rm_b}{1 - m_b}\right)^2 \left(1 + \frac{2m}{(1 - m)\phi^{1/3}}\right)^2,$$

563 where R is a constant equal to 2 indicating the additional distance traveled by the fluid as a
 564 function of the thickness of cementation. The volume fraction of pore-bridging cement is
 565 $m_b = P_b(1 - \phi_o)/\phi_o$, and the volume fraction of pore-filling cement is $m = P_f(1 - \phi_o)/\phi_o$.
 566 (ϕ_o is the original porosity of the sandstone grains, before compaction and cementation.)

567 For an unconsolidated sand of variable sizes, the specific surface area is

$$568 \quad a_u = \frac{6(\sigma^2 + \bar{D}^2)}{\gamma\sigma^3 + 3\bar{D}\sigma^2 + \bar{D}^3}$$

569 After cementation, the effective specific surface area follows the equation

$$570 \quad a_e = a_u \frac{1 - \phi_u}{1 - \phi} + a_b P_b + a_f P_f$$

571 where a_u is the specific surface area for an unconsolidated, uncemented sand, ϕ_o is the
 572 porosity of an unconsolidated sand, a_b is the specific surface area for a pore-bridging
 573 cement, a_f is the specific surface area for a pore-filling cement, and P_b, P_f are the relative
 574 fractions of pore-bridging and pore-filling cement, respectively.

575 Taking these equations together, the equation for permeability becomes

$$576 \quad k = \left[\bar{D}^2 \phi^3 (\gamma C_D^3 + 3C_D^2 + 1)^2 \right] \left\{ 2\tau_e (1 - \phi)^2 \left[6(1 + C_D^2) \frac{1 - \phi_u}{1 - \phi} + (a_b P_b + a_f P_f) \bar{D} (\gamma C_D^3 + 3C_D^2 + 1) \right]^2 \right\}^{-1}$$

577 Now, with these calculations, the properties of the grain size distribution measured by
 578 Ehrenberg (1990) can be used to test the theory derived by Panda and Lake (1995).

579 **Appendix C: Lognormal distribution statistics**

580 In this appendix we relate median grain size and the Trask Sorting Coefficient (S_o) to the
581 mean, standard deviation, and skewness of the grain size distribution. From the mean and
582 standard deviation, the coefficient of variation, $C_v = \bar{D}/\sigma$, can be calculated.

583 Grain size distribution is often described by the median grain size and the Trask Sorting
584 Coefficient (S_o), which is defined by $S_o = \sqrt{D_{0.75}/D_{0.25}}$, where D_p is the quantile value
585 indicated by p , such that $D_{0.25}$ is the 25%-ile grain size. Panda (1994, Appendix B) derived
586 an equation relating average grain size, Trask Sorting Coefficient, and the standard
587 deviation of the grain size, which is

588 This equation assumes that D_p is calculated from the distribution of grain sizes in \log_2
589 space, but most calculations of S_o use the definition provided above, so this should be re-
590 derived.

591 A new derivation, assuming lognormaly distributed grain sizes, can be described with the
592 PDF

593 the mean grain size is $\bar{D} = \exp(\mu + \sigma/2)$, and in terms of the median and Trask sorting
594 coefficient, the parameters of the distribution are

$$\begin{aligned} \mu &= \ln D_{0.5} \\ \sigma &= \frac{\ln S_o}{\sqrt{2} \operatorname{erf}^{-1}(0.5)} \end{aligned}$$

596 Simple R code to test these statistics is given below. It generates numbers from a random
597 lognormal distribution:

```

598 mu <- 3.14159
599 sigma <- 1
600 d <- rlnorm(10000, mu, sigma) # distribution of 1k points with mu=pi, sigma=1
601
602 trask <- sqrt(quantile(d,0.75) / quantile(d,0.25))
603 d_50 <- median(d)
604 mu_calc <- log(d_50)
605 erfinv <- function(x) qnorm((x + 1)/2)/sqrt(2)
606 sigma_calc <- log(trask) / (sqrt(2) * erfinv(0.5))
607 mean_calc <- exp(log(d_50) + sigma_calc/2)
608 exponent_thingie <- (2*sqrt(2) * erfinv(0.5))
609
610 cat(
611   "\nThe median is", round(median(d),1),
612     ". It should be", round(exp(mu),1),
613     "\nThe mean is",round(mean(d),1),
614     ". It should be", round(exp(mu + sigma/2),1),
615     "\nThe standard deviation is",round(sd(d),1),
616     ". It should be",round( sqrt( (exp(sigma^2)-1) * exp(2*mu+sigma^2))),
617     "\nThe Trask sorting coefficient is",round(sqrt(quantile(d,0.75) / quan
618 tile(d,0.25)),2),
619     ". \nFrom the Trask and median diameters, the mean should be", round(mean_c
620 alc,1),"or",
621     round(d_50 * trask^(1/(2*sqrt(2) * erfinv(0.5))),1),
622     ". \nThis is a deviation of", round((exp(mu + sigma/2) - mean_calc)/exp(mu

```

```

623 + sigma/2)*100,1),"percent\n"
624
625 )
626 ##
627 ## The median is 23 . It should be 23.1
628 ## The mean is 38.3 . It should be 38.2
629 ## The standard deviation is 50.8 . It should be 50
630 ## The Trask sorting coefficient is 1.96 .
631 ## From the Trask and median diameters, the mean should be 37.9 or 37.9 .
632 ## This is a deviation of 0.6 percent

```

633 The mean grain size can be calculated from the median grain size and standard deviation
634 through the equation (assuming a lognormal distribution of the grain size). In addition, the
635 coefficient of variation and skewness can be calculated. The equations for these terms are

$$\begin{aligned}
\bar{D} &= \exp[\ln(D_{0.5}) + \sigma/2] \\
&= D_{0.5} S_o^{1/(2\sqrt{2} \operatorname{erf}^{-1}(0.5))} \\
&= D_{0.5} S_o^{1.349} \\
C_D &= \sqrt{e^{\sigma^2} - 1} \\
&= \sqrt{e^{2.198(\ln S_o)^2} - 1} \\
\gamma &= (e^{\sigma^2} + 2)\sqrt{e^{\sigma^2} - 1} \\
&= (e^{\sigma^2} + 2)C_D \\
&= (e^{2.198(\ln S_o)^2} + 2)\sqrt{e^{2.198(\ln S_o)^2} - 1}
\end{aligned}$$

637 These equations are used in this manuscript to determine the Carman Kozeny coefficients
638 for each sample.